ELSEVIER

Journal of Molecular Structure: THEOCHEM 814 (2007) 61–73

THEO CHEM

www.elsevier.com/locate/theochem

Thermal rearrangement of 2-acetoxy-2,6,6-trimethylbicyclo[3.1.0]hexane: Theoretical elucidation of the mechanism

Safiye Sağ Erdem [a,*], Fahriye Uyar [a], Özlem Karahan [a], Kemal Yelekçi [b]

[a] *Chemistry Department, Marmara University, Faculty of Arts and Sciences, 34722, Göztepe, Istanbul, Turkey*
[b] *Kadir Has University, Faculty of Arts and Sciences, 34230, Fatih, Istanbul, Turkey*

Received 19 January 2007; accepted 22 February 2007
Available online 2 March 2007

Abstract

Bicyclohexenes are believed to be the immediate precursors of aromatic compounds. As a part of the exploratory study of thermal aromatization reactions, 2,6,6-trimethylbicyclo[3.1.0]hexan-2-ol and its ester derivative 2-acetoxy-2,6,6-trimethylbicyclo[3.1.0]hexane were synthesized. Pyrolysis of 2-acetoxy-2,6,6-trimethylbicyclo[3.1.0]hexane at 350 °C gave 1,3,3-trimethyl-1,4-cyclohexadiene instead of the expected product, 2,6,6-trimethylbicyclo[3.1.0]hex-2-ene. Computational methods such as PM3, HF/6-31G*, B3LYP/6-31G*, UHF/6-31G*, UB3LYP/6-31G*, and UMP2/6-31G* were employed in order to elucidate the mechanism of this reaction. The Gibbs free energy of activation and the reaction energy were calculated for the proposed polar and biradical mechanisms. The results showed that a two-step mechanism is plausible at 350 °C in which the expected product 2,6,6-trimethylbicyclo[3.1.0]hex-2-ene is the intermediate. The first step is the 1,2-elimination of the ester, leading to 2,6,6-trimethylbicyclo[3.1.0]hex-2-ene. The second step is the sigmatropic rearrangement of 2,6,6-trimethylbicyclo[3.1.0]hex-2-ene via concerted homodienyl 1,5-hydrogen shift, which is also the rate-determining step. UB3LYP/6-31G* calculations reveal that the cyclopropyl moiety of bicyclo[3.1.0]hex-2-ene can undergo homolytic bond cleavage to give an allylically stabilized biradical intermediate. However, the formation of 1,4-cyclohexadiene from such an intermediate through a biradical transition state involving 1,2-hydrogen migration does not seem to be plausible.

Keywords: Diradical intermediates; Singlet diradicals; Reaction profile; Bicyclic alkenes; Spin density

1. Introduction

The bicyclo[3.1.0]hexane system and its analogues have been the subject of numerous computational and experimental studies because of their strain energy and interesting ring-opening and skeletal-ring-rearrangement reactions [1–3]. Research on alkene analogs of these systems is also important especially for the petroleum industry, because such bicyclic alkenes can produce aromatic compounds at high temperatures. Theoretical studies on the thermal isomerization of bicyclo[3.1.0]hex-2-ene have also attracted much attention recently, because this system is an ideal model for studying degenerate rearrangement involving the continuous biradical transition state [4–6].

The pyrolysis of bicyclo[3.1.0]hex-2-ene in the range 314–347 °C in a flow system affords cyclohexadienes, benzene, and hydrogen [7]. Skeletal rearrangement occurs at the bicyclo ring system and may occur by one or both of two "ring walk" sequences. In order to gain insight into the thermal aromatization of this bicyclic system, a series of bicyclo[3.1.0]hexene derivatives were synthesized, and their pyrolysis reactions were studied in previous investigations [8,9]. Along this line, 2-acetoxy-2,6,6-trimethylbicyclo[3.1.0]hexane **1** was synthesized as a precursor of 2,6,6-trimethylbicyclo[3.1.0]hex-2-ene and then pyrolyzed. To our surprise, pyrolysis of **1** in a flow system at 350 °C gave

* Corresponding author. Tel.: +90 216 3479641; fax: +90 216 3478783.
E-mail addresses: erdem@marmara.edu.tr, erdem@anarad.org (S.S. Erdem).

0166-1280/$ - see front matter © 2007 Elsevier B.V. All rights reserved.
doi:10.1016/j.theochem.2007.02.041

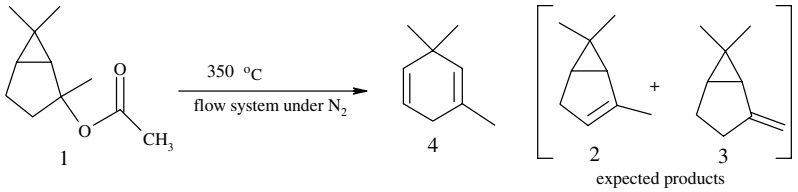

Scheme 1. Pyrolysis of **1**.

1,3,3-trimethyl-1,4-cyclohexadiene **4** instead of the expected bicyclic alkene products **2** and **3**, as shown in Scheme 1.

Along with these experimental findings, computational investigation of the conversion mechanism of compound **1**–**4** will be discussed in this paper.

We proposed several mechanisms for the reaction shown in Scheme 1. Mechanism I (Scheme 2) and Mechanism II (Scheme 3) were formulated to take into account the possibility that the expected bicyclohexene products **2** and **3** could be the intermediates of the thermal rearrangement leading to **4**. Both of these mechanisms involve two steps. The first step is the ester pyrolysis of the initial compound **1** to give the expected products **2** or **3**, and the second step is the 1,5-homodienyl hydrogen shift to produce the observed product **4**. Mechanisms III and IV (Schemes 4 and 5) were formulated to take into account the possibility of formation of biradical intermediates during the reaction, because various biradicals are believed to appear in the course of thermal aromatization reactions [7,9,10]. In addition, biradical intermediates and transition structures are also proposed to explain the thermal rearrangement mech-

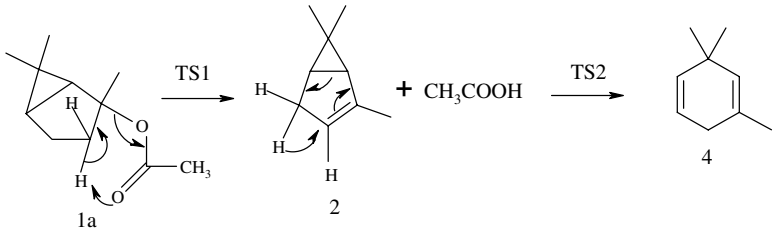

Scheme 2. Mechanism I.

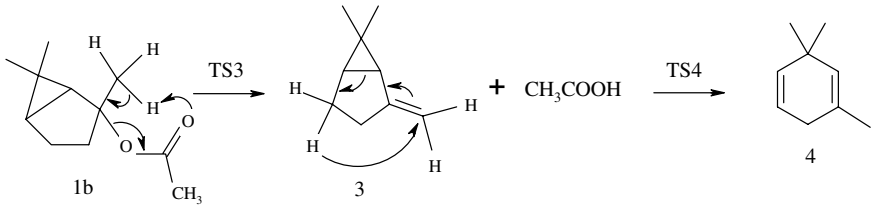

Scheme 3. Mechanism II.

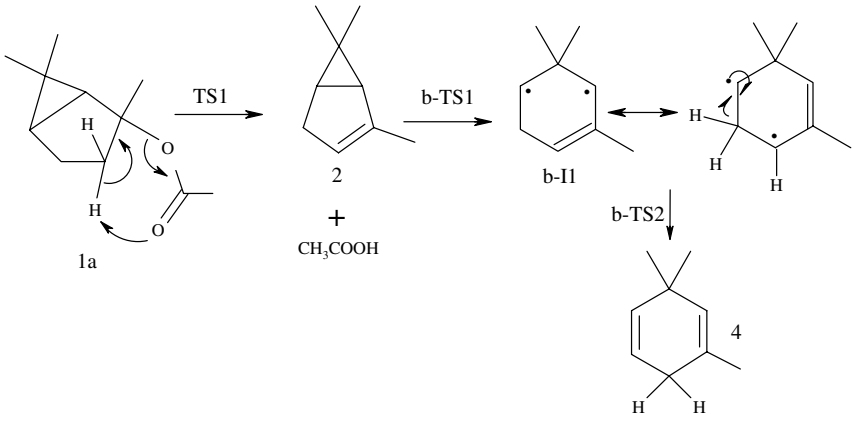

Scheme 4. Mechanism III.

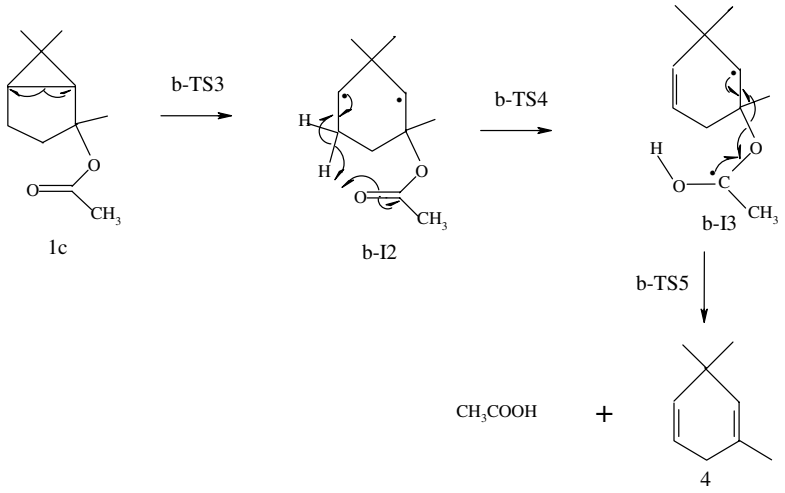

Scheme 5. Mechanism IV.

anism of various bicyclic structures [11–16]. Mechanistic studies on such systems are important because controversies over whether the mechanisms of potentially pericyclic reactions are concerted or stepwise can be resolved with a better understanding of biradical mechanisms.

Furthermore, we also considered concerted γ-elimination or 1,3-elimination mechanisms involving the heterolytic or homolytic cleavage of the bridgehead bond. While β-eliminations (1,2-eliminations) are well-known reactions, γ-eliminations are more complex and uncommon. There are only a few examples of such reactions in the literature [17]. In parallel to this, all our attempts to locate transition structures connecting the reactants and the products failed.

Computational methods were employed to generate reaction profiles of the possible reaction pathways (Mechanism I, II, III, and IV) and to understand which one of them is a plausible mechanism.

2. Methods and materials

2.1. Computational details

The Gaussian 98 program package [18] was used for all calculations. Geometries of the reactants, products, and transition states were fully optimized with the semiempirical PM3, HF/6-31G*, and B3LYP/6-31G* (Becke's three parameter exchange functional with the Lee-Yang-Parr correlation functional) methods for the closed-shell systems and with UHF/6-31G*, UB3LYP/6-31G*, and UMP2/6-31G* for biradical structures. In biradical mechanisms, the change in multiplicity along the reaction path is spin-forbidden and is usually a slow process. Assuming no change in electron spin, the electronic state of the biradical structures is open-shell singlet. The keyword guess = (mix, always) in Gaussian 98 was utilized to optimize singlet biradical structures. Internal stability of the wavefunctions was checked by stability calculations. Vibrational frequencies were calculated at the PM3, HF/6-31G*, B3LYP/6-31G* and UHF/6-31G*, and UB3LYP/6-31G* levels to determine whether the optimized structures corresponded to local minima on the potential energy surface or the transition states. Transition structures were characterized with one imaginary frequency corresponding to the stretching motion of the bonds being broken or formed. Intrinsic reaction coordinate analysis (IRC) [19] was carried out on the transition structures to confirm that they led to the desired reactants and products. These reactants and products were further subjected to full geometry optimization. Thermodynamic calculations were performed at two different temperatures, 25 and 350 °C. Thermal corrections were included by using the freq(ReadIso,ReadFC) keyword; and thermal energies, enthalpies, and Gibbs free energies were calculated for all stationary points. From this data, activation energies and reaction energies were evaluated.

2.2. Experimental

Elemental analysis was performed by Galbraith Laboratories, Knoxville, TN. Infrared spectra were recorded with a Perkin-Elmer Model 237 or a Sargent Welch Model 3-200 infrared spectrophotometer. NMR spectra were determined with a JEOL FX 90 Q spectrometer, with $CDCl_3$ as solvent and TMS as internal standard. All ^{13}C NMR spectra are noise-decoupled.

2.2.1. 2,6,6-Trimethylbicyclo[3.1.0]hexan-2-ol (*6*)

First, 5-Methyl-4-hexenoic acid was synthesized with the minor modification of the reported procedure by Julia and Listrumelle [20] and then converted to the corresponding acid chloride. The acid chloride was reacted with diazomethane in ether at 0 °C to give 1-diazo-6-methyl-5-hepten-2-one [8]. Cyclization of the diazoketone was accomplished in the presence of metallic copper powder and anhydrous copper sulfate by using cyclohexane as solvent. Distillation of the residue (b.p. 60 °C, 5 mmHg) afforded the pure product **5**. The overall yield was 40% for three steps. υ_{max}(film)/

cm^{-1} 1725 (C=O). δ_H(100 MHz; $CDCl_3$; Me_4Si) 1.14 (6 H s, b, Me, Me), 1.4–1.19 (6 H, m). δ_C(100 MHz; $CDCl_3$; Me_4Si) 212.54 (C=O), 39.59, 36.23, 33.71, 25.56, 24.05, 17.92, 14.20. Ketone **5** was converted to alcohol **6** by a standard Grignard reaction procedure. The crude product was further purified by sublimation at 75–80 °C (2 mm Hg) to afford 2 g (78% yield) of pure product **6**, m.p. 55.0 °C. (Found C, 76.87; H, 11.35 $C_9H_{16}O$ requires C, 77.09; H, 11.49 %). υ_{max}(in CCl_4)/cm^{-1} 3400 (–OH, s, b), 3020 (s), 2875 (s), 1455 (m), 1376 (m), 1150 (s). δ_H(100 MHz; $CDCl_3$; Me_4Si) 1.83–1.60 (5H, m), 1.38 (3H, s), 1.30 (3H, s), 1.04 (2H, d), 0.97 (3H, s). δ_C(100 MHz; $CDCl_3$; Me_4Si) 81.38 (C-2), 41.19, 40.60, 31,59, 30.78, 28.92, 23.92, 19.97, 16.25.

2.2.2. 2-Acetoxy-2,6,6-Trimethylbicyclo[3.1.0]hexane (*1*)

In a three-necked flask equipped with a condenser and a stirrer were placed 1.08 g (7.70 mmol) alcohol **6**, 1.48 g acetic anhydride, 1.08 cm^3 triethylamine, 6 cm^3 CH_2Cl_2, and 24.5 mg 4-dimethylaminopyridine. The reaction mixture was stirred for 20 h at room temperature and poured into 70 cm^3 hexane. The organic layer was separated and washed with 5% HCl, saturated $NaHCO_3$, and brine solutions successively. The solution was dried over $MgSO_4$, and the solvent was removed by rotary evaporation to yield 1.00 g product (71%). The IR spectrum of the residue showed the disappearance of the alcohol group and the presence of an ester carbonyl band at 1750 cm^{-1}. υ_{max}(in CCl_4)/cm^{-1} 2950 (s), 2850 (s), 1750 (s), 1375 (s), 1260 (s), 1150 (s), 1075 (s), 955 (s), 880 (s). δ_H(100 MHz; $CDCl_3$; Me_4Si) 1.97–1.14 (15H, m), 0.969 (3H, s). δ_C(100 MHz; $CDCl_3$; Me_4Si) 170.06 (C=O), 90.41(C-2), 39.62 (COMe), 31.00, 28.52, 27.55, 23.04, 22.06, 20.26, 15.83, 14.10.

2.2.3. 1,3,3-Trimethyl-1,4-cyclohexadiene (*4*)

The acetate **1** was pyrolyzed at 350 °C in a flow system by using prepurified N_2 as the carrier gas. The pyrolysate was collected in a receiver which was cooled in an ice bath. The product was washed successively with water, saturated $NaHCO_3$, and water several times. The organic phase was dried over $CaCl_2$, and the product was separated by preparative VPC (10% Carbowax 20 M on Cromosorb G). The product was identified as 1,3,3-trimethyl-1,4-cyclohexadiene on the basis of its ^1H and ^{13}C NMR spectra. δ_H(100 MHz; $CDCl_3$; Me_4Si) 5.02 (1H, s), 4.64 (2H, s, b), 3.24 (2H, s, b), 1.67 (3H, m), 1.16 (6H, d). δ_C(100 MHz; $CDCl_3$; Me_4Si) 149.76, 141.46, 127.22, 108.25, 53.04, 36.68, 30.28, 20.48, 16.63.

3. Results and discussion

3.1. Mechanisms I and II

3.1.1. Structural aspects

For Mechanism I, three-dimensional pictures of the optimized structures are given in Fig. 1. **TS1** is the transition state of the pyrolysis step in which the σ bonds C3–H14, C2–O10 and the π bond between C11 and O12 break, while the O12–H14 bond and the π bonds C11–O10 and C2–C3 form to give the endocyclic bicycloalkene **2**. The second step is the 1,5 sigmatropic migration of H16 from C4 to C3 with concomitant cleavage of the C1–C5 bond belonging to the cyclopropyl fragment, which can be observed in the structure of the second transition state, **TS2**. Other examples of such 1,5-homodienyl hydrogen shifts have appeared in the literature [21–26] and are known to be stereospecific [24–26].

For Mechanism II, three-dimensional pictures of the optimized structures are given in Fig. 2. **TS3** is the transition state of the pyrolysis step in which O12 abstracts H18 to produce the exocyclic bicycloalkene **3**. **TS4** is the transition state of the second step, in which H17 migrates from C4 to C9 to form product **4**. In **TS4**, the cyclohexadiene ring is distorted to a boat-like structure to afford the migration of H17 to C9. In contrast to this, in the second step of Mechanism I, **TS2** adopts a nearly planar structure.

For the pyrolysis step of both mechanisms, the PM3 method predicts a later transition state than the one predicted by the HF and DFT methods. This is observed from the longer C3–H14 (**TS1**) or C9–H18 (**TS3**) bonds and shorter O12–H14 (**TS1**) or O12–H18 bonds in the PM3 than the bond lengths obtained from HF and DFT calculations. The Cartesian coordinates of all of the optimized transition structures are given in Supplementary material.

3.1.2. Energetical aspects

Energies of all optimized structures are tabulated in Supplementary material. For each step, the reaction energy (ΔE_1 or ΔE_2) and the activation energy ($\Delta E^{\#}$) were calculated at 350 °C in terms of electronic energy (E_e), thermal energy (E), enthalpy (H), and Gibbs free energy (G). The results are given in Tables 1 and 2, and the energy profiles are shown in Fig. 3.

The three standard computational methods can be compared in terms of the reaction energies and the activation energies in Tables 1 and 2. The semiempirical PM3 method, which is the least reliable of the three, overestimates the exothermicity of ester pyrolysis (Step 1) relative to the HF and DFT results. However, it predicts reaction energies (ΔE_2) that are similar to the HF and DFT values for the sigmatropic hydrogen shift (Step 2). The ΔE_1 and ΔE_2 values calculated by the HF and DFT theories are in agreement within 2–4 kcal/mol.

For both mechanisms, ΔE_1, calculated with all three methods in terms of Gibbs free energy, exhibits an increase in exothermicity with respect to the values in terms of E_e, E, and H. This is due to the increase in entropy because the molecularity increases as 2-acetoxy-2,6,6-trimethylbicyclo[3.1.0]hexane is pyrolyzed to bicyclic alkenes and acetic acid in Step 1. This entropy effect lowers the Gibbs free energy of the products with respect to the reactant.

According to Gibbs free energy values, both Step 1 and Step 2 are exothermic for each mechanism. However, Step 1 of Mechanism I is about 4 kcal/mol more exother-

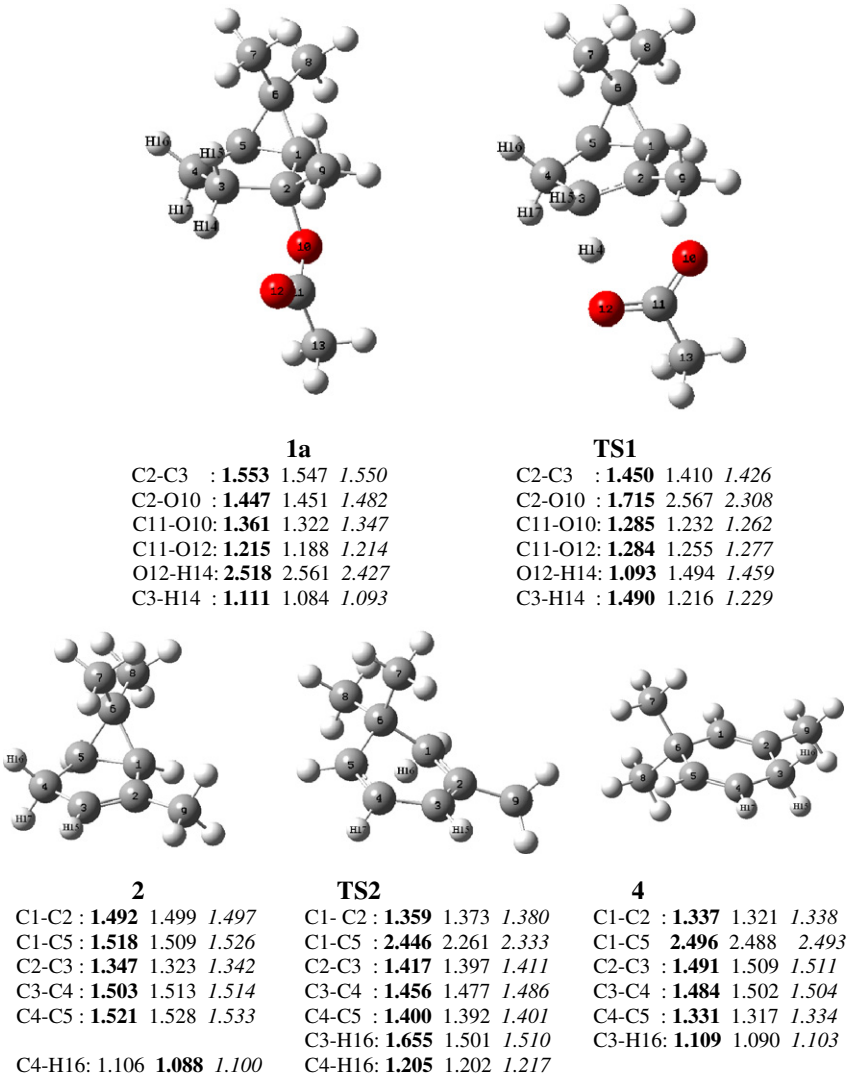

1a

C2-C3 : **1.553** 1.547 *1.550*
C2-O10 : **1.447** 1.451 *1.482*
C11-O10: **1.361** 1.322 *1.347*
C11-O12: **1.215** 1.188 *1.214*
O12-H14: **2.518** 2.561 *2.427*
C3-H14 : **1.111** 1.084 *1.093*

TS1

C2-C3 : **1.450** 1.410 *1.426*
C2-O10 : **1.715** 2.567 *2.308*
C11-O10: **1.285** 1.232 *1.262*
C11-O12: **1.284** 1.255 *1.277*
O12-H14: **1.093** 1.494 *1.459*
C3-H14 : **1.490** 1.216 *1.229*

2

C1-C2 : **1.492** 1.499 *1.497*
C1-C5 : **1.518** 1.509 *1.526*
C2-C3 : **1.347** 1.323 *1.342*
C3-C4 : **1.503** 1.513 *1.514*
C4-C5 : **1.521** 1.528 *1.533*
C4-H16: 1.106 **1.088** *1.100*

TS2

C1- C2 : **1.359** 1.373 *1.380*
C1-C5 : **2.446** 2.261 *2.333*
C2-C3 : **1.417** 1.397 *1.411*
C3-C4 : **1.456** 1.477 *1.486*
C4-C5 : **1.400** 1.392 *1.401*
C3-H16: **1.655** 1.501 *1.510*
C4-H16: **1.205** 1.202 *1.217*

4

C1-C2 : **1.337** 1.321 *1.338*
C1-C5 **2.496** 2.488 *2.493*
C2-C3 : **1.491** 1.509 *1.511*
C3-C4 : **1.484** 1.502 *1.504*
C4-C5 : **1.331** 1.317 *1.334*
C3-H16: **1.109** 1.090 *1.103*

Fig. 1. Important distances (Å) in the optimized structures of Mechanism I calculated with the PM3 (bold), HF/6-31G* (normal), and B3LYP/6-31G* (italic) methods.

mic than Step 1 of Mechanism II, whereas Step 2 of Mechanism I liberates 4 kcal/mol less energy than Step 2 of Mechanism II. This is because the bicyclic intermediate of Mechanism II, consisting of a less substituted double bond, is 4.09 kcal/mol less stable (i.e. according to B3LYP/6-31G*) than the intermediate produced in Mechanism I.

Taylor [27] measured the rate of pyrolysis for various esters at temperatures between 522 and 606 K. Depending on the type of ester, the activation energies ranged between 34.7 and 47.8 kcal/mol. The activation energy for the pyrolysis of ethyl formate was predicted by nineteen different computational methods [28], including semiempirical, density-functional, Hartree–Fock, and post-Hartree–Fock treatments with various basis sets. Comparison of the experimental activation energy of ethyl formate (40–44 kcal/mol) with those of calculated values shows that, in general, Hartree–Fock and semiempirical theories overestimate the activation barrier, whereas density functional methods predict values very close to the experimental measurements. From our results in Tables 1 and 2, a similar situation is observed for the pyrolysis of 2-acetoxy-2,6,6-trimethylbicyclo[3.1.0]hexane **1**. Unfortunately, there is no experimental measurement for its activation barrier. However, computed values from semiempirical PM3 and HF/6-31G* theories are much higher than the value predicted by DFT, B3LYP/6-31G*, as in the case of ethyl formate. PM3 and HF/6-31G* values are in good agreement with each other for the pyrolysis of 2-acetoxy-2,6,6-trimethylbicyclo[3.1.0]hexane. The activation energies of the pyrolysis step for Mechanism I and Mechanism II were calculated to be very close. For example, the Gibbs free energy of activation varies by only 0.46–3.12 kcal/mol, depending on the computational method used. Calculated activation energies for the pyrolysis steps are within the range of the measured energies for various esters reported by Taylor [27]. Thus, the first steps of both mechanisms are expected to occur readily.

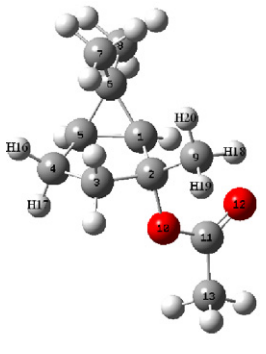

1b

C2-C9 : **1.525** 1.523 *1.527*
C2-C10 : **1.449** 1.454 *1.484*
C11-O10: **1.360** 1.322 *1.348*
C11-O12: **1.216** 1.190 *1.213*
O12-H18: **2.531** 2.463 *2.436*
C9-H18 : **1.098** 1.085 *1.096*

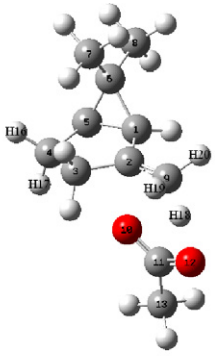

TS3

C2-C9 : **1.429** 1.410 *1.425*
C2-O10 : **1.732** 2.712 *2.403*
C11-O10: **1.287** 1.231 *1.262*
C11-O12: **1.281** 1.255 *1.274*
O12-H18: **1.114** 1.486 *1.505*
C9-H18 : **1.456** 1.222 *1.209*

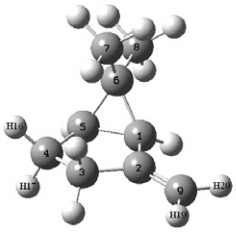

3

C2-C9 : **1.328** 1.319 *1.336*
C1-C2 : **1.483** 1.493 *1.490*
C1-C5 : **1.510** 1.508 *1.525*
C4-C5 : **1.513** 1.525 *1.529*
C4-H17: **1.105** 1.084 *1.096*

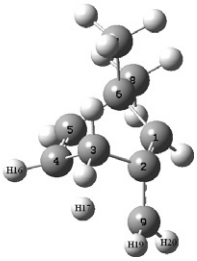

TS4

C2-C9 : **1.390** 1.400 *1.417*
C1-C2 : **1.390** 1.372 *1.379*
C1-C5 : **2.202** 2.136 *2.224*
C4-C5 : **1.421** 1.402 *1.410*
C4-H17: **1.318** 1.411 *1.394*
C9-H17: **1.782** 1.658 *1.659*

Fig. 2. Important distances (Å) in the optimized structures of Mechanism II calculated with the PM3 (bold), HF/6-31G* (normal), and B3LYP/6-31G* (italic) methods.

For both mechanisms, Step 2 exhibits a much higher activation energy than Step 1. Therefore, the homodienyl hydrogen-shift reaction is the rate-determining step. The comparison of $\Delta E_2^{\#}$ values in Tables 1 and 2 reveals that Mechanism II is unfavorable since it exhibits 20–32 kcal/mol higher activation energy (depending on the computational method used) than Mechanism I. This is an expected result because **TS4** is highly unstable owing to its boat-like distorted structure as we discussed earlier. It is interesting that, for the homodienyl hydrogen-shift, PM3 predicts much closer activation barrier to that of B3LYP/6-31G* whereas HF/6-31G* overestimates the barrier by about 22–29 kcal/mol relative to B3LYP/6-31G*.

The homodienyl hydrogen-shift rearrangement or retro-ene reaction was investigated experimentally for 1,1-dimethyl-2-alkenyl cyclopropanes by Berson et al. [24,26], for 1-(fluoromethyl)-2-vinylcyclopropane by Dolbier et al. [29], and for vinylaziridines by Ahman and Somfai [30]. In these reports, the activation energies of such rearrangements occurring in non-bicyclic structures vary between 31.1 and 42.2 kcal/mol in a temperature range of 193–270 °C. According to the computational work on 1-methyl-2-vinylcyclopropane by Loncharich and Houk [25] with the HF/3-21G basis set, the activation energies for the endo and exo transition structures are 48.8 and 65.9 kcal/mol, respectively, favoring the endo mode of reaction. An experimental study on the bicyclic system bicyclo[3.1.0]hex-2-ene was reported by Glass et al. [22]. They observed no isomerization after 68 h at 220 °C, indicating $\Delta H^{\#} > 44$ kcal/mol at this temperature. However, in the range 314-347 °C, bicyclo[3.1.0]hex-2-ene yielded two primary products, cyclohexa-1,4- and 1,3-diene, with an activation energy of 50.2 kcal/mol [7]. This value is in excellent agreement with the activation energy (51.7 kcal/mol) of homodienyl 1,5-hydrogen shift for Mechanism I

Table 1
Activation energies ($\Delta E^{\#}$) and reaction energies (ΔE) in terms of electronic energy (E_e), electronic energy including the zero-point energy correction (E_{e+ZPE}), thermal energy (E^{350}), enthalpy (H^{350}), and Gibbs free energy (G^{350}) calculated for Mechanism I at 350 °C in kcal/mol

	Method	E_e	E_{e+ZPE}	E^{350}	H^{350}	G^{350}
Step 1						
$\Delta E_1^{\#}$	PM3	48.6684	44.6667	44.6329	44.7288	44.0360
	HF/6-31G*	48.8737	43.1870	44.0643	44.0643	38.4839
	B3LYP/6-31G*	35.8889	31.4503	31.6354	31.6354	29.5263
ΔE_1						
	PM3	0.5764	−1.9490	−2.6568	−1.4194	−31.0443
	HF/6-31G*	9.5074	6.4632	5.4021	6.6402	−21.6048
	B3LYP/6-31G*	12.2390	9.5781	8.1355	9.3735	−17.0535
Step 2						
$\Delta E_2^{\#}$	PM3	54.7061	50.7572	51.2579	51.2579	49.4708
	HF/6-31G*	78.6120	74.4942	74.7396	74.7390	74.2489
	B3LYP/6-31G*	56.3953	52.3918	52.7733	52.7733	51.6947
ΔE_2						
	PM3	−14.7678	−15.3147	−14.9050	−14.9050	−16.6274
	HF/6-31G*	−13.2819	−13.4121	−13.1411	−13.1411	−14.2436
	B3LYP/6-31G*	−10.9909	−11.1299	−10.8714	−10.8714	−12.0473

Table 2
Activation energies ($\Delta E^{\#}$) and reaction energies (ΔE) in terms of electronic energy (E_e), electronic energy including the zero-point energy correction (E_{e+ZPE}), thermal energy (E^{350}), enthalpy (H^{350}), and Gibbs free energy (G^{350}) calculated for Mechanism II at 350 °C in kcal/mol

	Method	E_e	E_{e+ZPE}	E^{350}	H^{350}	G^{350}
Step 1						
$\Delta E_1^{\#}$	PM3	52.6530	47.7408	47.8399	47.8406	46.7769
	HF/6-31G*	51.5154	45.8840	44.8850	44.8850	41.6070
	B3LYP/6-31G*	38.3503	33.9050	34.1761	34.1761	29.0670
ΔE_1						
	PM3	2.3963	−0.2491	−1.3648	−0.1267	−27.7003
	HF/6-31G*	14.4748	11.8440	10.5143	11.7524	−15.8079
	B3LYP/6-31G*	16.7209	14.0817	12.7068	13.9443	−13.6976
Step 2						
$\Delta E_2^{\#}$	PM3	83.7866	80.0721	79.7878	79.7878	81.4532
	HF/6-31G*	102.2403	98.3104	97.8354	97.8354	100.2581
	B3LYP/6-31G*	73.0281	69.3362	68.8179	68.8185	71.6008
ΔE_2						
	PM3	−16.6820	−17.1313	−16.3702	−16.3702	−19.8879
	HF/6-31G*	−16.7551	−17.2826	−16.8602	−16.8602	−17.9283
	B3LYP/6-31G*	−15.0795	−15.4885	−15.1503	−15.1497	−16.1091

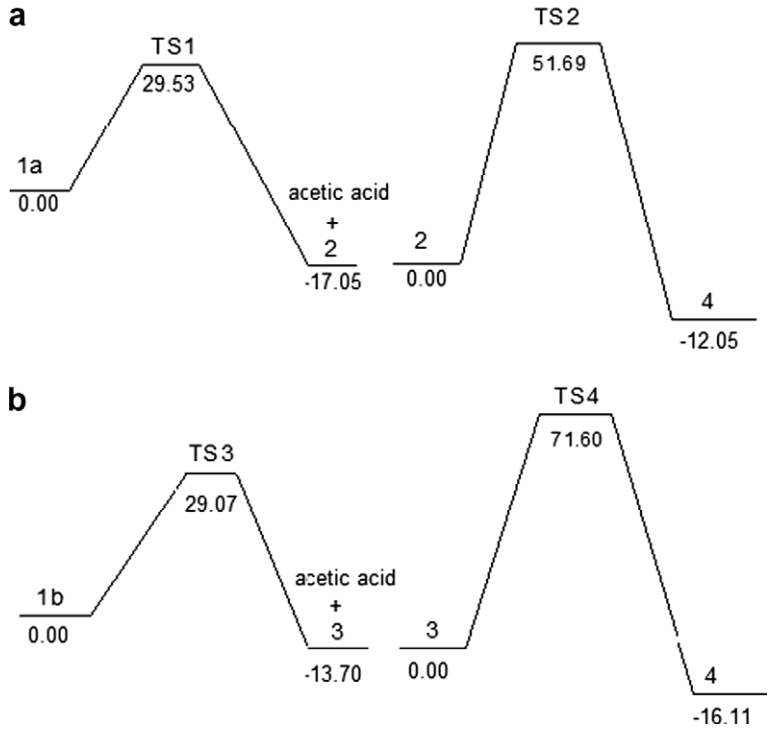

Fig. 3. The B3LYP/6-31G* energy profile for (a) Mechanism I and (b) Mechanism II. Energies are from G^{350} values in kcal/mol.

calculated with the B3LYP/6-31G* method. On the other hand, for the thermal isomerization of bicyclo[3.1.0]hex-2-ene, Ellis and Frey [7] proposed a 1,2-hydrogen shift through biradical intermediates, which will be discussed in the next section. George et al. [31] investigated the homodienyl 1,5-hydrogen shift on a larger bicyclic system, bicyclo[5.1.0]octa-2,4-diene and its 8-oxa derivative by ab initio molecular orbital theory. They reported activation energies of 26.9 and 26.3 kcal/mol for these two compounds, respectively, as a result of MP2/6-31G*//RHF/6-31G* level calculations at 298 K. To the best of our knowledge, no theoretical work has been reported in the literature for the homodienyl 1,5 hydrogen shift in bicyclohexenes.

3.2. Biradical mechanisms

3.2.1. Structural aspects

Mechanism III in Scheme 4 was proposed to account for the further rearrangement of compound **2** through biradical intermediate **b-I1**. This mechanism involves three steps: Step 1 is the 1,2-elimination of ester **1a** and is the same as

that in Mechanism I. Step 2 is the homolytic dissociation of bridgehead bond via the biradical transition structure **b-TS1**, leading to the allylically stabilized biradical intermediate, **b-I1**. Step 3 involves 1,2-hydrogen migration to the carbon atom, which is part of the allylic system. Three-dimensional pictures and the critical distances of the optimized structures related to Step 2 and Step 3 are given in Fig. 4. Structural parameters and $\langle S^2 \rangle$ values of **b-TS1** and **b-I1**, calculated by UB3LYP/6-31G*, are in good agreement with the reported values on the parent molecule bicyclo[3.1.0]hex-2-ene [4]. For **b-TS1**, the C1–C5 distance predicted by UB3LYP/6-31G* is 0.39 Å longer than that predicted by UHF/6-31G*. Thus, it is a later transition state and resembles the biradical intermediate **b-I1**. For **b-TS1**, atomic spin densities (see Supplementary material) calculated from UHF/6-31G* are equally high on C1 and C5, indicating the homolytic dissociation of the C1–C5 bond. In addition, C2 and C3 exhibit spin densities lower than the ones on C1 and C5 as a result of the allylic delocalization. Spin densities of **b-TS1** from UB3LYP are not equally distributed on C1 and C5 as a result of its product-like character. Distribution of the spin density is very similar to **b-I1**. It is mostly located on C5 and slightly delocalized on C1, C2, and C3. For Step 3, UB3LYP/6-31G* calculations did not produce any transition state with biradical character. In all our attempts, the $\langle S^2 \rangle$ value became zero and UB3LYP solutions collapsed into the restricted B3LYP solutions after a few steps. In order to understand if this is related to the basis set used (6-31G*), we repeated the UB3LYP calculations by using the basis set 6-31G** to add polarization to the hydrogen atoms, and the basis set 6-31+G** to add diffusion functions. Both calculations produced zero for the $\langle S^2 \rangle$ value. This situation may arise from the fact that UB3LYP predicts a much lower spin density on C3 of **b-I1** than the UHF and UMP2 methods. This reveals that contamination from higher spin states is probably larger in UHF and UMP2 calculations. In connection with this, UHF/6-31G* and UMP2/6-31G* optimizations did produce the planar transition state **b-TS2** as shown in Fig. 4. The structure of **b-TS2** obtained from UMP2/6-31G* is very similar to that obtained from UHF/6-31G*. The C4–H16 bond is broken as the C3–H16 bond is formed in a nonsynchronous manner. Both methods predict a larger spin density on C3 than on C4, which is in accordance with the longer C3–H16 distance relative to C4–H16.

Mechanism IV in Scheme 5 accounts for the homolytic cleavage of the C1–C5 bond prior to the abstraction of H17 by O12 of ester **1c**. Overall, it is a 1,3-elimination which requires the **1c** conformation of 2-acetoxy-2,6,6-trimethylbicyclo[3.1.0]hexane. The reaction involves three main steps. However, conformational change is also necessary to convert the product of **b-TS4** to **b-I3**, which can be seen from the 3-D structures given in Fig. 5. Alterations in critical distances and the atomic spin densities confirm the characterization of the optimized structures.

3.2.2. Energetical aspects

Energies of all the optimized structures involved in biradical mechanisms were tabulated and given as Supplementary material. For each step, the reaction energy (ΔE) and the activation energy ($\Delta E^{\#}$) were calculated at 350 °C in terms of electronic energy (E_e), thermal energy (E), enthalpy (H), and Gibbs free energy (G). The results are given in Tables 3 and 4, and the energy profiles are shown in Figs. 6 and 7. It is a challenging task to compute the values for the singlet biradical species because it requires high-level calculations. In the literature, computational studies of these systems are limited to small molecules up to six C atoms [4,32–34]. For a reliable prediction of the structures and properties of such species, a preferable theoretical method is the complete active space SCF (CASSCF) method. Currently, we do not have the resources to carry out the calculations by this method. On the other hand, the DFT formalism appears to account well for nondynamical and dynamical correlation effects that are not included in single-determinant HF theory [35]. A computational exploration of the vinylcyclopropane-cyclopentene rearrangement involving biradical transition states [34] reports that UB3LYP/6-31G* underestimates the energy barrier by

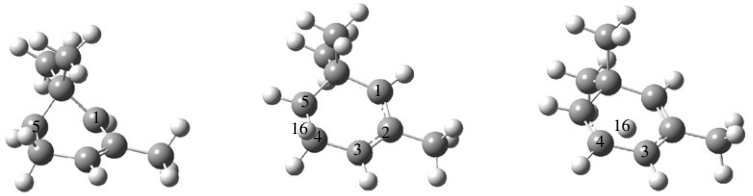

b-TS1 **b-I1** **b-TS2**

C1-C5:	2.015	*2.405*	C1-C5:	2.483	*2.489*	1.461		
C1-C2:	1.457	*1.403*	C1-C2:	1.396	*1.392*	1.381	C1-C2: 1.366	1.344
C2-C3:	1.351	*1.383*	C2-C3:	1.391	*1.390*	1.380	C2-C3: 1.432	1.422
C4-C5:	1.509	*1.492*	C4-C5:	1.503	*1.495*	1.494	C4-C5: 1.402	1.402
			C4-H16:	1.094	*1.110*	1.108	C4-H16: 1.292	1.216
							C3-H16: 1.401	1.474

Fig. 4. Important distances (Å) in the optimized structures of Mechanism III calculated with the UHF/6-31G* (normal), UB3LYP/6-31G* (italic), and UMP2/6-31G* (underlined) methods.

only 6 kcal/mol, and it reproduces the general trend in the barrier heights correctly. In addition, Balcioglu and Özsar [36] applied UB3LYP/6-31G* calculations to the thermal conversion of 1,3-hexadien-5-yne to benzene which also involves biradical 1,2 H-shifts, and the calculations gave excellent agreement with available experimental energy values. Therefore, in the present study, we aimed at optimizing the structures of the open-shell singlet species with UB3LYP/6-31G*. First, UHF/6-31G* calculations were performed to obtain the initial geometries for UB3LYP/6-31G* and for the purpose of comparison.

For Mechanism III, activation energies and reaction energies are given in Table 3. Step 1 of this mechanism is the same as that in Mechanism I (Table 1). Step 1 and Step 3 are exothermic, whereas Step 2 is endothermic. According to B3LYP/6-31G* calculations, the Gibbs free energy of activation for the pyrolysis step (Step 1) is 29.53 kcal/mol. The reaction profile for Step 2 and Step 3 is shown in Fig. 6. It is expected that the UB3LYP/6-31G* method predicts activation energies more accurately than UHF/6-31G*. Thus, it is observed that UHF/6-31G* underestimates the homolytic bond dissociation (Step 2) barrier by 12 kcal/mol and the reaction energy by 24 kcal/mol. Energies related to 1,2-hydrogen migration (Step 3) are evaluated by using the UMP2/6-31G* and UHF/6-31G* methods, because UB3LYP/6-31G* did not produce a singlet biradical transition state as discussed above. Considering the UHF/6-31G* values, Step 3 exhibits the highest barrier and is the rate-determining step. As it is observed in Fig. 6, **b-TS2** is a highly unstable structure and lies 79.44 and 49.09 kcal/mol higher in energy than intermediate **2** according to UMP2/6-31G* and UHF/6-31G*, respectively. Thus, the UHF/6-31G* method also underestimates the energy of the transition structure for 1,2-hydrogen migration in comparison to UMP2/6-31G*. Because Step 2 is highly endothermic, no energy can be supplied from this step to reach the transition state **b-TS2**. Considering this and the fact that UB3LYP/6-31G* produced no **b-TS2**, it seems that 1,2-hydrogen migration is not a plausible reaction. Moreover, when the energy profiles of Mechanism I and Mechanism III are compared in Fig. 6, it is observed that Mechanism I exhibits a lower energy barrier and is expected to occur faster than Mechanism III. It is possible that the reaction overcomes the energy barrier from **2** to biradical intermediate **b-I1** but, the reverse activation energy for this step is very low and **b-I1** will eventually return to **2**, which will then undergo a 1,5-homodienyl hydrogen shift.

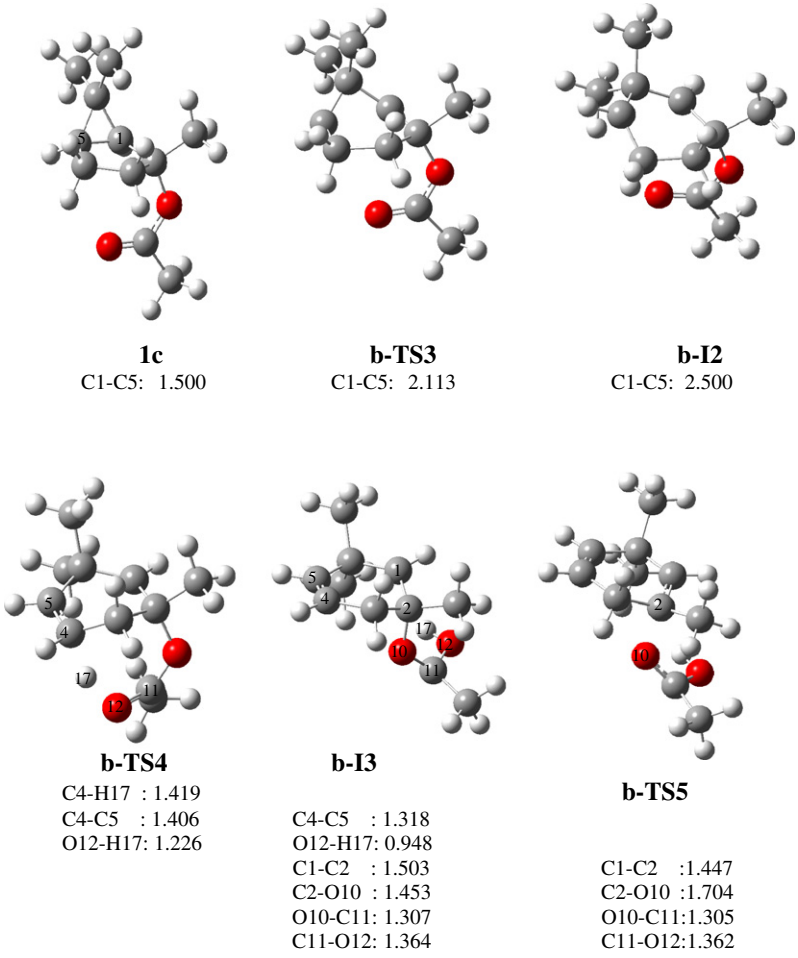

Fig. 5. Important distances (Å) in the optimized structures of Mechanism IV calculated with the UHF/6-31G method.

Table 3
Activation energies ($\Delta E^{\#}$) and reaction energies (ΔE) in terms of electronic energy (E_e), electronic energy including the zero-point energy correction (E_{e+ZPE}), thermal energy (E^{350}), enthalpy (H^{350}), and Gibbs free energy (G^{350}) calculated for Mechanism III at 350 °C in kcal/mol

	Method	E_e	E_{e+ZPE}	E^{350}	H^{350}	G^{350}
Step 2						
$\Delta E_2^{\#}$	UHF/6-31G*	26.9207	23.3060	23.8011	23.8011	22.7575
	UB3LYP/6-31G*	40.0044	36.3304	36.9830	36.9830	34.5470
ΔE_2	UHF/6-31G*	15.5313	11.5309	13.2704	13.2704	6.8536
	UB3LYP/6-31G*	39.2816	36.0009	37.5659	37.5659	31.4271
Step 3						
$\Delta E_3^{\#}$	UHF/6-31G*	42.2203	39.6749	38.9320	38.9320	42.2420
	UB3LYP/6-31G*					
	UMP2/6-31G*	25.7823	23.2365[a]			30.2965[b]
ΔE_3	UHF/6-31G*	−28.8133	−24.9444	−26.4115	−26.4115	−21.0972
	UB3LYP/6-31G*	−50.2727	−47.1309	−48.4374	−48.4374	−43.4745

[a] The ZPE correction was used from UHF/6-31G* calculations.
[b] The Gibbs free energy correction was used from UHF/6-31G* calculations.

Table 4
Activation energies ($\Delta E^{\#}$) and reaction energies (ΔE) in terms of electronic energy (E_e), electronic energy including the zero-point energy correction (E_{e+ZPE}), thermal energy (E^{350}), enthalpy (H^{350}), and Gibbs free energy (G^{350}) calculated for Mechanism IV at 350 °C in kcal/mol with the UHF/6-31G* method

	E_e	E_{e+ZPE}	E^{350}	H^{350}	G^{350}
Step 1					
$\Delta E_1^{\#}$	34.3500	30.7826	31.4001	31.4001	29.8389
ΔE_1	31.0749	27.2850	28.9284	28.9284	23.5275
Step 2					
$\Delta E_2^{\#}$	72.6646	67.8315	67.3069	67.3069	71.4635
ΔE_2	30.8785	31.3336	31.3273	31.3273	33.3133
Step 3					
$\Delta E_3^{\#}$	5.9553	4.7357	4.3787	4.3787	4.2526
ΔE_3	−65.7280	−65.5668	−67.9940	−66.7560	−92.6893

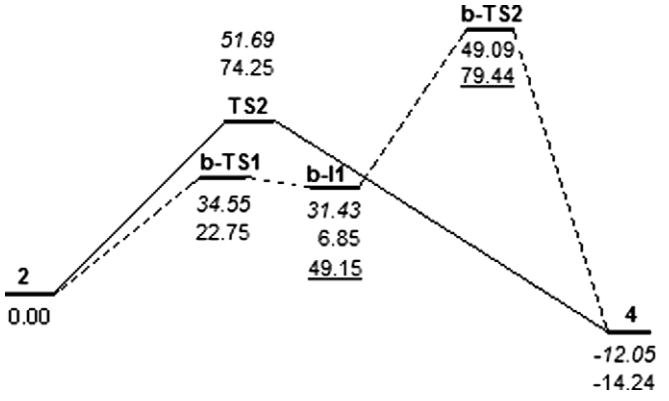

Fig. 6. Energy profiles for Step 2 of Mechanism I (——) and Step 2 and Step 3 of Mechanism III (-----). Energies are from G^{350} values in kcal/mol calculated with the UB3LYP/6-31G* (italic), UHF/6-31G* (normal), and UMP2/6-31G* (underlined) methods.

An analogous case of Mechanism III was also considered, in which bicyclic alkene **3** undergoes first a homolytic dissociation of the C1–C5 bond and then a 1,4-hydrogen migration from C4 to the exocyclic C9. The homolytic bond dissociation step produced the same activation energy for Mechanism III, but we observed that it is almost impossible to obtain a transition structure for 1,4-hydrogen migration because the molecule must be extremely distorted to a bent structure to afford this migration. Therefore, no transition structure could be obtained.

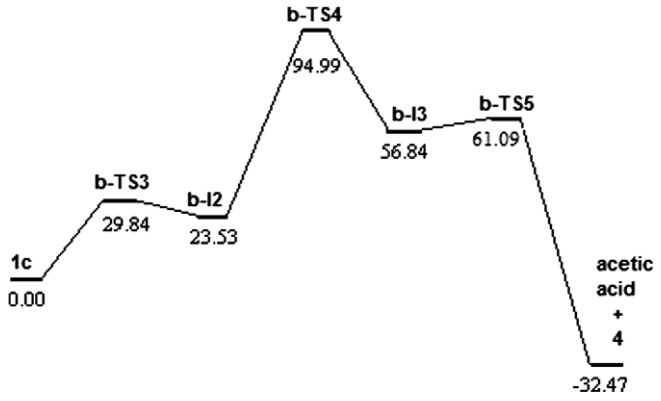

Fig. 7. The UHF/6-31G* energy profile for Mechanism IV. Energies are from G^{350} values in kcal/mol.

Thermal isomerization of bicyclo[3.1.0]hex-2-ene, the prototype of compound **2**, was investigated by Ellis and Frey [7] in the gas phase, in the range 313–347 °C. The reaction is unimolecular and yields two primary products, cyclohexa-1,3- and 1,4-diene. In the temperature range studied, the 1,3-diene is thermally stable, but the 1,4-diene decomposes to benzene, probably by a one-stage elimination of molecular hydrogen from the two *gem*-hydrogen atoms at C3 and C6 of the cyclohexa-1,4-diene. A two-step biradical mechanism was proposed for the formation of cyclohexa-1,3- and 1,4-diene at this temperature. Similar to Mechanism III, the first step is the dissociation of the bridgehead bond in the bicyclic compound, and the second step is a 1,2- or 1,4-hydrogen shift to give the cyclohexa-

1,4- and 1,3-dienes, respectively. Since, in our case, the C6 of 2,6,6-trimethylbicyclo[3.1.0]hex-2-ene, **2**, is occupied by two methyl groups, hydrogen migration is not possible from this position. As a result, 1,3-diene and benzene cannot form. The 1,2-migration of hydrogen from C4 is possible, which results in the formation of 1,4-diene. However, as discussed above, 1,2-hydrogen migration involving a biradical transition state does not seem to take place in our case. We thought that methyl groups in compound **2** might exert steric constraint and block the reaction. Therefore, we wanted to check whether 1,2-hydrogen migration was possible for the prototype compound bicyclo[3.1.0]hex-2-ene, which has no substituents. Transition-state optimizations with UB3LYP/6-31G* and UB3LYP/6-31+G** calculations again collapsed into the restricted B3LYP solution, producing the same result as that for compound **2**. In order to gain more insight into the nature of the transition structure obtained from this optimization, the reaction path was followed by IRC calculations in both directions. This procedure has proved that the transition structure indeed corresponds to the homodienyl 1,5-hydrogen shift, connecting bicyclo[3.1.0]hex-2-ene to 1,4-cyclohexadiene as in the second step of Mechanism I. This reveals that the conclusion drawn from the study on 2,6,6-trimethylbicyclo[3.1.0]hex-2-ene is likely to be of general significance for such bicyclic structures.

For Mechanism IV, activation energies and reaction energies were calculated with UHF/6-31G* and are given in Table 4. Step 1 and Step 2 are endothermic, whereas Step 3 is exothermic. Step 2 exhibits the highest activation energy (71.46 kcal/mol) and is the rate-determining step. The reaction profile is shown in Fig. 7. The transition structure of Step 2, **b-TS4**, is 95 kcal higher in energy than the reactant and therefore it is extremely unstable. We attempted to optimize this transition structure with UB3LYP/6-31G*, but the SCF calculation did not converge and gave an unreasonable structure. On the other hand, our experience from the calculations on Mechanism III indicates that UHF/6-31G* underestimates the activation energy of the reactions involving singlet biradicals. Since the barrier (71.46 kcal/mol) calculated by UHF/6-31G* is already very high, UB3LYP/6-31G* is expected to produce an even higher activation energy. This reasoning and the unsuccessful optimization of **b-TS4** with UB3LYP/6-31G* reveals that this mechanism is not likely to occur. Therefore, UB3LYP/6-31G* calculations were not performed for the remaining structures of this mechanism.

3.3. Comments on the synthesis of the compounds

2-Acetoxy-2,6,6-trimethylbicyclo[3.1.0]hexane **1** was prepared as shown in Scheme 6. Compound **5** was synthesized by starting from 5-methyl-4-hexenoic acid in three steps [8]. Cyclization of diazoketone was accomplished in the presence of metallic copper and various copper salts. The best result was obtained in the presence of copper powder and anhydrous copper sulfate by using cyclohexane as solvent. The overall yield for three steps (chlorination, diazotization and cyclization) was 40%. Its structure was characterized by comparing the obtained spectroscopic data with the reported values [20,37]. Compound **5** was used as a precursor for the synthesis of compound **6**. The Grignard reaction went smoothly, and the methylation was accomplished in 78% yield. The structure of this new compound was fully identified by its spectroscopic and elemental analysis data. The corresponding ^{1}H NMR, ^{13}C NMR, IR, and elemental analysis results were consistent with the structure of the anticipated product. Conversion of alcohol **6** to its acetoxy compound **1** was carried out in 71% yield. ^{1}H NMR, ^{13}C NMR, and IR spectra obtained for this compound proved the disappearance of the alcohol moiety and the formation of the acetate product. Finally, pyrolysis of acetate **1** in a flow system gave the rearranged 1,3,3-trimethyl-1,4-cyclohexadiene product **4** as a major product instead of the desired bicyclic alkene 2,6,6-trimethylbicyclo[3.1.0]hex-2-ene. Preparative vapor-phase chromatography results showed predominantly one major peak and a few minor peaks. The major peak was carefully collected and analyzed on the basis of its ^{1}H NMR and ^{13}C NMR spectra. Additional support was also obtained by comparing the spectra of 1,3,3-trimethyl-1,4-cyclohexadiene to the reported spectra of 2,6,6-trimethyl-1,3-cyclohexadiene [38]. Allylic and vinylic hydrogen atoms of 1,3,3-

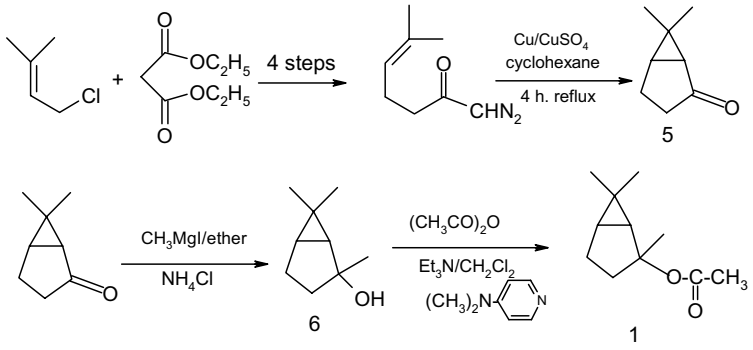

Scheme 6. Synthesis of **1**.

trimethyl-1,4-cyclohexadiene were centered at $\delta = 3.24$ and 4.64–5.02, respectively, whereas allylic and vinylic hydrogen atoms of 2,6,6-trimethyl-1,3-cyclohexadiene were centered at $\delta = 2.06$ and 5.75–5.20, respectively. Doubly bonded carbons of 1,3,3-trimethyl-1,4-cyclohexadiene appeared at $\delta = 108.25$–149.76, while those of 2,6,6-trimethyl-1,3-cyclohexadiene were much closer to each other (at $\delta = 125.4$–132.1) because of the delocalization of the π electrons. These spectroscopic data were supported by the computationally generated spectra of compound **4** by Gaussian [18] and also by analogous spectra of known compounds [39].

4. Conclusions

Synthesis of 2-acetoxy-2,6,6-trimethylbicyclo[3.1.0]hexane **1** was accomplished in a series of reactions. FVP of **1** gave 1,3,3-trimethyl-1,4-cyclohexadiene **4** in a flow system under N_2 at 350 °C. Possible thermal rearrangement mechanisms of **1** to give **4** were investigated by using computational methods.

Calculations on biradical mechanisms generated high activation energies, and some of the transition structures could not be optimized. Among all the mechanisms considered, Mechanism I was the one found to occur the most readily. The first step liberates 17.05 kcal/mol of energy, and the reaction can use this energy in order to overcome the barrier in the rate-determining step. The calculated activation energy of the rate-determining step is in good agreement with the measured activation energy reported in the literature for the rearrangement of bicyclo[3.1.0]hex-2-ene, which is the prototype of **2**. UB3LYP calculations reveal that the thermal rearrangement of bicyclo[3.1.0]hex-2-ene to 1,4-cyclohexadiene does not involve a 1,2-hydrogen shift with biradical character. Instead, an orbital-symmetry-allowed mechanism, which involves synchronous cleavage of the cyclopropane ring and 1,5-hydrogen shift, takes place readily. This result will be of interest to many other mechanistic studies related with thermal rearrangement and isomerization of bicyclohexenes, because various singlet biradicals are proposed in such systems, and it is extremely difficult to isolate and characterize these structures by using experimental techniques. Besides, it resolves the controversy over the concerted 1,5-hydrogen shift versus stepwise biradical mechanism in the analogous systems, which has been a topic of debate for more than forty years [7,21,39,40]. It is also useful to other theoretical studies on similar mechanisms, because it compares several computational methods and gives an idea about their weak and strong points.

Furthermore, this work reports the elegant, modified synthesis of 6,6-dimethylbicyclo[3.1.0]hex-2-one (**5**). Transformation of this compound to a new compound 2,6,6-trimethylbicyclo[3.1.0]hexan-2-ol (**6**) via Grignard conditions is another accomplishment on this susceptible ring system. Finally, synthesis and pyrolysis of 2-acetoxy-2,6,6-trimethylbicyclo[3.1.0]hexane (**1**), and the computational investigation of this reaction provide new insights into the thermal rearrangement mechanism of this type of bicyclic ring systems.

Acknowledgments

This work was supported by Marmara University, Scientific Research Project Commission, Project No.: BSE-086/051201. The experimental work was carried out at Ohio University. K.Y. is very grateful to Prof. W.D. Huntsman for his guidance and for providing his laboratory facilities. S.S.E. is grateful to Prof. N. Balcioglu for his help.

Appendix A. Supplementary data

Supplementary data associated with this article can be found, in the online version, at doi:10.1016/j.theochem.2007.02.041.

References

[1] H. Pines, The Chemistry of Catalytic Hydrocarbon Conversions, Academic Press, New York, 1981 (Chapter 4).
[2] R.W. Dolbier, J.J. Keaffaber, R.C. Burkholder, F.S. Sellers, H. Koroniak, J. Pradhan, Tetrahedron Lett. 32 (1991) 3933.
[3] Y.H. Lee, Y. Kim, H.Y. Lee, G.B. Kim, Tetrahedron Lett. 42 (2001) 7431.
[4] C.P. Suhrada, K.N. Houk, J. Am. Chem. Soc. 124 (2002) 8796.
[5] C. Doubleday, C.P. Suhrada, K.N. Houk, J. Am. Chem. Soc. 128 (2006) 90.
[6] W.vonE. Doering, T. Zhang, E.K.G. Schmidt, J. Org. Chem. 71 (2006) 5688.
[7] J.R. Ellis, M.H. Frey, J. Chem. Soc. (A) (1966) 553.
[8] K. Yelekçi, Ph.D. Thesis, Ohio University, 1987.
[9] W.D. Huntsman, J.P. Chen, K. Yelekçi, T.K. Yin, L.J. Zhang, J. Org. Chem. 53 (1988) 4357.
[10] W.R. Dolbier Jr., J.J. Keaffaber, C.R. Burkholder, S.F. Sellers, H. Koroniak, J. Pradhan, Tetrahedron Lett. 32 (1991) 3933.
[11] P.B. Shevlin, M.L. McKee, J. Am. Chem. Soc. 110 (1988) 1666.
[12] D. Hasselmann, Angew. Chem. Int. Ed. 14 (1975) 257.
[13] B.K. Carpenter, J. Am. Chem. Soc. 118 (1996) 10329.
[14] J.E. Baldwin, E.J. Keliher, J. Am. Chem. Soc. 124 (2002) 380.
[15] J.E. Baldwin, P.A. Leber, Tetrahedron Lett. 42 (2001) 195.
[16] C.P. Suhrada, C. Selçuki, M. Nendel, C. Cannizzaro, K.N. Houk, P.-J. Rissing, D. Baumann, D. Hasselmann, Angew. Chem. Int. Ed. 44 (23) (2005) 3548.
[17] D. Beruben, H. Marek, J. Norman, N. Platzer, Tetrahedron Lett. 34 (1993) 7575;
M.N.T. Chang, C.T. Walsh, J. Am. Chem. Soc. 103 (1981) 4921;
W.L. Parker, R.B. Woodward, J. Org. Chem. 34 (1969) 3085;
M. Sugawara, J. Yoshida, J. Org. Chem. 65 (2000) 3135;
J. Boyd, K.H. Overton, J. Chem. Soc. Perkin Trans. I 20 (1972) 2533.
[18] M.J. Frisch, G.W. Trucks, H.B. Schlegel, G.E. Scuseria, M.A. Robb, J.R. Cheeseman, V.G. Zakrzewski, J.A. Montgomery Jr., R.E. Stratmann, J.C. Burant, S. Dapprich, J.M. Millam, A.D. Daniels, K.N. Kudin, M.C. Strain, O. Farkas, J. Tomasi, V. Barone, M. Cossi, R. Cammi, B. Mennucci, C. Pomelli, C. Adamo, S. Clifford, J. Ochterski, G.A. Petersson, P.Y. Ayala, Q. Cui, K. Morokuma, D.K. Malick, A.D. Rabuck, K. Raghavachari, J.B. Foresman, J. Cioslowski, J.V. Ortiz, A.G. Baboul, B.B. Stefanov, G. Liu, A. Liashenko, P. Piskorz, I. Komaromi, R. Gomperts, R.L. Martin, D.J. Fox, T. Keith, M.A. Al-Laham, C.Y. Peng, A. Nanayakkara, M. Challa-

combe, P.M.W. Gill, B. Johnson, W. Chen, M.W. Wong, J.L. Andres, C. Gonzalez, M. Head-Gordon, E.S. Replogle, and J.A. Pople, Gaussian, Inc., Pittsburgh PA, 1998.
[19] C. Gonzalez, H.B. Schlegel, J. Chem. Phys. 90 (1989) 2154; C. Gonzalez, H.B. Schlegel, J. Phys. Chem. 94 (1990) 5523.
[20] S. Julia, G. Listrumelle, Bull. Soc. Chim. Fr. (1966) 3490.
[21] R.J. Ellis, H.M. Frey, J. Chem. Soc. Suppl. 1 (1964) 5578.
[22] D.S. Glass, R.S. Boikess, S. Winstein, Tetrahedron Lett. 10 (1966) 999.
[23] J.K. Crandall, R.J. Watkins, Tetrahedron Lett. 18 (1967) 1717.
[24] J.P. Daub, J.A. Berson, Tetrahedron Lett. 25 (1984) 4463.
[25] R.J. Loncharich, K.N. Houk, J. Am. Chem. Soc. 110 (1988) 2089.
[26] P.A. Parziale, J.A. Berson, J. Am. Chem. Soc. 112 (1990) 1650.
[27] R. Taylor, J. Chem. Soc. Perkin Trans. II 10 (1975) 1025; H.B. Amin, R. Taylor, J. Chem. Soc. Perkin Trans. II 15 (1975) 1802; R. Taylor, J. Chem. Soc. Perkin Trans. II 12 (1979) 1730.
[28] W.J. Hehre, A Guide to Molecular Mechanics and Quantum Chemical Calculations, Wavefunctions, Inc., Irvine, 2003, p. 293.
[29] W.R. Dolbier Jr., A.C. Alty, O. Phanstiel, J. Am. Chem. Soc. 109 (1987) 3046.
[30] J. Ahman, P. Somfai, Tetrahedron 55 (1999) 11595.
[31] P. George, C.W. Bock, J.P. Glusker, A. Greenberg, J.D. Gallagher, J. Org. Chem. 60 (1995) 4385.
[32] R. Liu, X. Zhou, T. Zuo, Chemical Physics Lett. 325 (2000) 457.
[33] K.N. Houk, M. Nendel, O. Wiest, J.W. Storer, J. Am. Chem. Soc. 119 (1997) 10545.
[34] M. Nendel, D. Sperling, O. Wiest, K.N. Houk, J. Org. Chem. 65 (2000) 3259.
[35] M.H. Lim, S.E. Worthington, F.J. Dulles, C.J. Cramer, Chemical Applications of Density Functional Theory ACS Symposium Series, 629 (1996) 402.
[36] N. Balcioglu, A.Ö. Özsar, J. Mol. Struct. (Theochem) 677 (2004) 125.
[37] D.A. Lightner, D.E. Jackman, Tetrahedron Lett. 35 (1975) 3051.
[38] S. Yao, M. Johannsen, R.G. Hazell, K.A. Jorgensen, J. Org. Chem. 63 (1998) 118.
[39] R.S. Cooke, U.H. Andrews, J. Org. Chem. 38 (1973) 2725.
[40] D.L. Garin, J.S. Chickos, J. Org. Chem. 45 (1980) 2721.